Electronic supplementary information

For

Pd^{II} insertion-triggered *meso*-carbon extrusion of N-fused pentaphyrin to form N-fused sapphyrin Pd^{II} complexes

Akito Nakai,[a] Tomoki Yoneda,[a] Takayuki Tanaka *[a] and Atsuhiro Osuka *[a]

[a]Department of Chemistry, Graduate School of Science, Kyoto University, Sakyo-ku, Kyoto 606-8502, Japan

E-mail: taka@kuchem.kyoto-u.ac.jp; osuka@kuchem.kyoto-u.ac.jp

Fax: +81-75-753-3970; Tel: +81-75-753-4007

Contents

1. General information

The chemicals used for synthesis were of reagent grade quality unless otherwise mentioned. Dry toluene was obtained by distillation over CaH_2. Dry THF was obtained by passing through alumina under N_2 in a solvent purification system. Thin-layer chromatography (TLC) was carried out on aluminum sheets coated with silica gel 60 F_{254} (Merck 5554). ^{1}H (600.17 MHz) and ^{19}F (564.73 MHz) NMR spectra were acquired on a JEOL ECA-600 spectrometer and chemical shifts were reported as the delta scale in ppm relative to $CHCl_3$ as internal references for ^{1}H (δ = 7.26 ppm) and hexafluorobenzene as an external reference for ^{19}F (δ = –162.9 ppm). Coupling constants (J) are given in Hz. High-Resolution Atmospheric-Pressure-Chemical-Ionization Time-Of-Flight (HR-APCI-TOF) mass spectra were recorded on a BRUKER Daltonics micrOTOF LC instrument. UV/Vis/NIR absorption spectra were recorded on a Shimadzu UV-3600PC spectrometer. Redox potentials were measured by cyclic voltammetry on ALS electrochemical analyzer model 612E. X-Ray single crystal diffraction analyses were performed on a Rigaku XtaLAB P200 apparatus at –180 °C using two-dimensional detector PILATUS 100K/R with Cu$K\alpha$ radiation (λ= 1.54187 Å). The structures were solved by direct method SHELEXT-2014/5 and refined by SHELEXL-2014/7 programs.[S1]

2. Synthetic procedures and compound data

N-Fused [22]sapphyrin Pd(II) complexes **5** and **6**

To a solution of **1** (62.1 mg, 51.1 μmol) in dry THF (50 mL) was added $Pd(tfa)_2$ (90.5 mg, 272 μmol, 5 eq.) and the resulting solution was stirred at 70 °C for 3 h. The reaction mixture was cooled to room temperature and passed through a short florisil column with dichloromethane. After removal of solvent, the residue was purified by silica-gel chromatography (C-400, dichloromethane : *n*-hexane = 1 : 2) to provide **5** as a brown fraction and **6** as a red fraction. Recrystallization from dichloromethane / *n*-hexane afforded **5** (23.5 mg, 20.6 μmol, 40%) and **6** (3.9 mg, 2.9 μmol, 6%).

Compound data of **5**

^{1}H NMR ($CDCl_3$, 298 K) δ [ppm] = 10.57 (s, 1H, NH), 10.31 (d, 1H, J = 4.8 Hz, β-H), 10.01 (d, 1H, J = 4.8 Hz, β-H), 9.31 (d, 1H, J = 4.8 Hz, β-H), 9.16 (d, 1H, J = 4.8 Hz, β-H), 8.96 (d, 1H, J = 4.8 Hz, β-H), 8.90 (d, 1H, J = 4.8 Hz, β-H), 8.88 (d, 1H, J = 4.8 Hz, β-H) and 8.75 (d, 1H, J = 4.8 Hz, β-H).

^{19}F NMR ($CDCl_3$, 298 K) δ [ppm] = –135.73 (d, 2F, J = 17.3 Hz, *o*-F), –136.47 (d, 2F, J = 17.3 Hz, *o*-F), –136.65 (d, 2F, J = 17.3 Hz, *o*-F), –140.19 (d, 2F, J = 17.3 Hz, *o*-F), –149.47 (t, 1F, J = 19.5 Hz, *p*-F), –151.78 (t, 1F, J = 21.7 Hz, *p*-F), –152.00 (t, 1F, J = 19.5 Hz, *p*-F), –152.76 (t, 1F, J = 21.7 Hz, *p*-F), –159.09 (t, 2F, J = 17.3 Hz, *m*-F), –159.80 (t, 2F, J = 17.3 Hz, *m*-F) and –161.56 (m, 4F, *m*-F).

UV/Vis/NIR (CH_2Cl_2): λ_{max} [nm] (ε [$M^{-1}cm^{-1}$]) = 459 (78000), 514 (76000), 633 (7400), 689 (11000) and 804 (5000).

HR APCI-TOF-MS (negative): *m*/*z* calcd for $C_{48}H_9F_{20}N_5{}^{106}Pd$: 1140.9595, $[M]^-$; found: 1140.9581.

Compound data of **6**

^{1}H NMR ($CDCl_3$, 298 K) δ [ppm] = 10.42 (d, 1H, J = 5.0 Hz, β-H), 10.04 (s, 1H, NH), 8.92 (s, 1H, β-H), 8.82 (d, 1H, J = 5.0 Hz, β-H), 8.78 (d, 1H, J = 5.0 Hz, β-H), 8.73 (d, 1H, J = 5.0 Hz, β-H), 8.71 (d, 1H, J = 5.0 Hz, β-H) and 8.61 (d, 1H, J = 5.0 Hz, β-H).

^{19}F NMR ($CDCl_3$, 298 K) δ [ppm] = –135.68 (d, 2F, J = 17.3 Hz, *o*-F), –136.47 (d, 2F, J = 17.3 Hz, *o*-F), –136.61 (d, 2F, J = 17.3 Hz, *o*-F), –139.51 (d, 2F, J = 17.3 Hz, *o*-F), –139.59 (d, 2F, J = 17.3 Hz, *o*-F), –148.74 (t, 1F, J = 19.5 Hz, *p*-F), –149.62 (t, 1F, J = 21.7 Hz, *p*-F), –150.94 (t, 1F, J = 19.5 Hz, *p*-F), –151.16 (t, 1F, J = 19.5 Hz, *p*-F), –151.54 (t, 1F, J = 21.7 Hz, *p*-F), –158.55 (t, 2F, J = 21.7 Hz, *m*-F), –159.10 (t, 2F, J = 17.3 Hz, *m*-F), –159.23 (t, 2F, J = 17.3 Hz, *m*-F) and –160.99 (m, 4F, *m*-F).

UV/Vis/NIR (CH_2Cl_2): λ_{max} [nm] (ε [$M^{-1}cm^{-1}$]) = 475 (49000), 545 (48000), 722 (12000) and 766 (7700).

HR APCI-TOF-MS (negative): *m*/*z* calcd for $C_{55}H_8F_{25}N_5O^{106}Pd$: 1334.9388, $[M]^-$; found:1334.9401.

Synthesis of dimer **7**

To a solution of **5** (82.1 mg, 72.0 μmol) in dry toluene (5 mL) were added DDQ (197.3 mg, 86.9 μmol, 1.2 eq) and $Sc(OTf)_3$ (241 mg, 49.0 μmol, 0.7 eq), and the resulting mixture was stirred at room temperature for 4 h. The solution was passed through an alumina column with dichloromethane as an eluent. The eluate was evaporated and purified by silica-gel column chromatography (C-400, dichloromethane : *n*-hexane = 1 : 3). Obtained red fraction was evaporated to afford **7** (20.2 mg, 8.9 μmol, 25%).

^{1}H NMR ($CDCl_3$, 298 K) δ [ppm] = 10.68 (s, 1H, NH), 10.46 (d, 1H, J = 5.0 Hz, β-H), 10.18 (d, 1H, J = 4.1 Hz, β-H), 9.76 (s, 1H, β-H), 9.28 (d, 1H, J = 5.0 Hz, β-H), 9.13 (d, 1H, J = 4.1 Hz, β-H), 8.97 (d, 1H, J = 5.0 Hz, β-H), 8.91 (m, 2H, β-H), 8.81 (d, 1H, J = 4.6 Hz, β-H), 8.77 (m, 2H, β-H), 8.70 (d, 1H, J = 4.6 Hz, β-H), 8.52 (d, 1H, J = 4.6 Hz, β-H), 8.26 (d, 1H, J = 4.6 Hz, β-H) and 7.98 (d, 1H, J = 5.5 Hz, β-H).
^{19}F NMR ($CDCl_3$, 298 K) δ [ppm] = –132.45 (d, 1F, J = 26.0 Hz, *o*-F), –133.98 (d, 1F, J = 26.0 Hz, *o*-F), –135.55 (d, 1F, J = 21.7 Hz, *o*-F), –135.75 (d, 1F, J = 21.7 Hz, *o*-F), –136.21 (d, 1F, J = 30.3 Hz, *o*-F), –136.30 (d, 2F, J = 21.7 Hz, *o*-F), –136.52 (d, 1F, J = 21.7 Hz, *o*-F), –136.65 (d, 1F, J = 21.7 Hz, *o*-F), –136.80 (d, 2F, J = 26.0 Hz, *o*-F), –137.18 (s, 1F, *o*-F), –138.26 (s, 1F, *o*-F), –139.31 (d, 1F, J = 26.0 Hz, *o*-F), –140.72 (d, 2F, J = 21.7 Hz, *o*-F), –148.96 (t, 1F, J = 21.7 Hz, *p*-F), –151.37 (t, 1F, J = 19.5 Hz, *p*-F), –151.62 (m, 3F, *p*-F), –151.92 (t, 1F, J = 19.5 Hz, *p*-F), –152.25 (t, 1F, J = 19.5 Hz, *p*-F), –153.08 (s, 1F, *p*-F), –158.71 (t, 1F, J = 23.8 Hz, *m*-F), –158.85 (t, 1F, J = 19.5 Hz, *m*-F), –159.22 (t, 2F, J = 19.5 Hz, *m*-F), –160.38 (t, 1F, J = 21.7 Hz, *m*-F), –161.18 (t, 1F, J = 17.3 Hz, *m*-F), –161.51~–161.33 (m, 5F, *m*-F), –161.68 (d, 1F, J = 13.0 Hz, *m*-F), –161.85 (t, 1F, J = 21.7 Hz, *m*-F), –162.10 (t, 1F, J = 23.8 Hz, *m*-F), –162.40 (t, 1F, J = 19.5 Hz, *m*-F) and –163.57 (t, 1F, J = 19.5 Hz, *m*-F).
UV/Vis/NIR (CH_2Cl_2): λ_{max} [nm] (ε [$M^{-1}cm^{-1}$]) = 457 (120000), 521 (120000), 638 (17000), 697 (21000) and 799 (13000).
HR APCI-TOF-MS (negative): m/z calcd for $C_{96}H_{16}F_{40}N_{10}{}^{106}Pd_2$: 2279.9035, $[M]^-$; found: 2279.9049.

3. NMR spectra

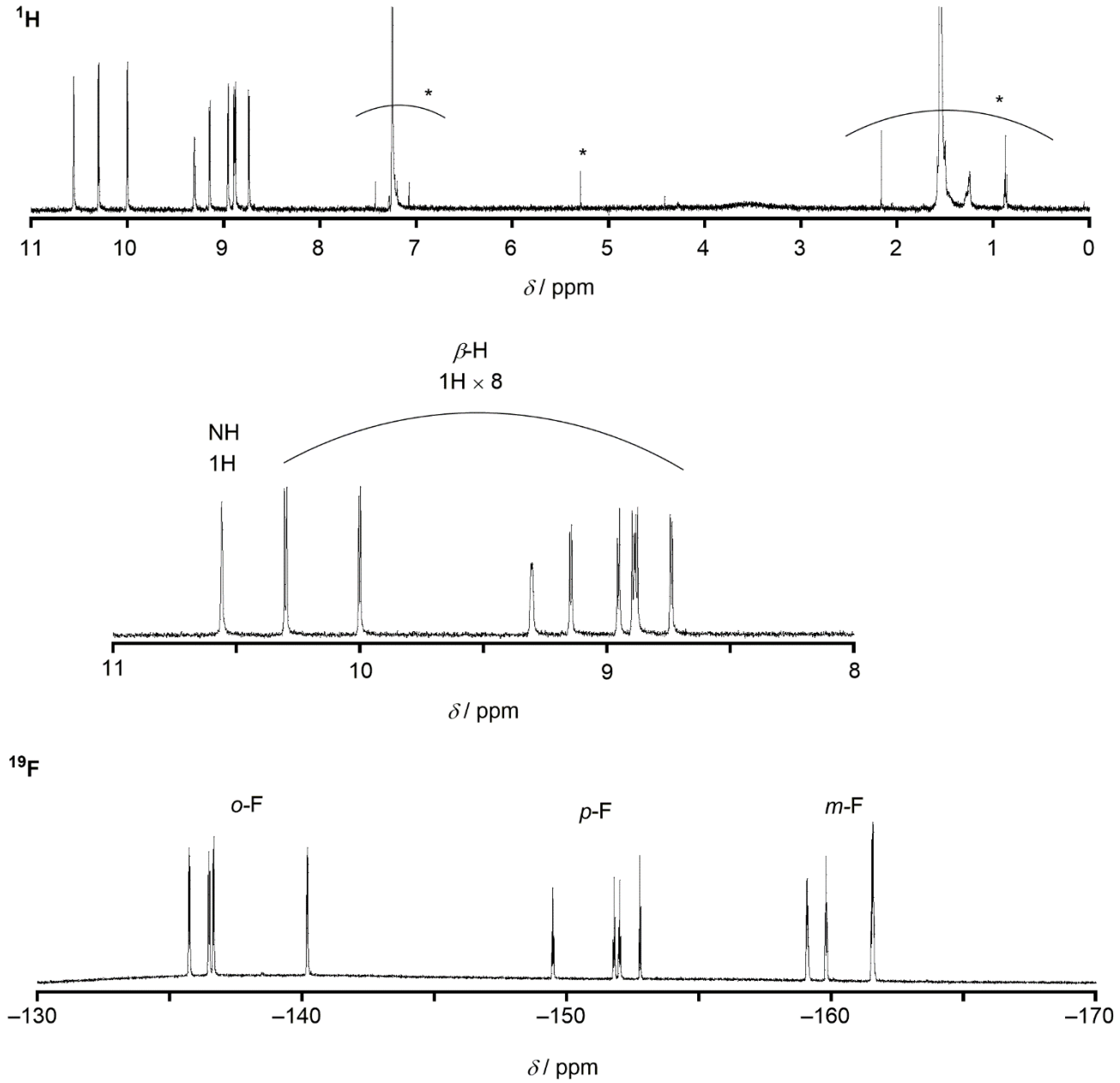

Fig. S1 ^{1}H and ^{19}F NMR spectra of **5** in $CDCl_3$ at room temperature. Peaks marked with * are due to residual solvents and impurities.

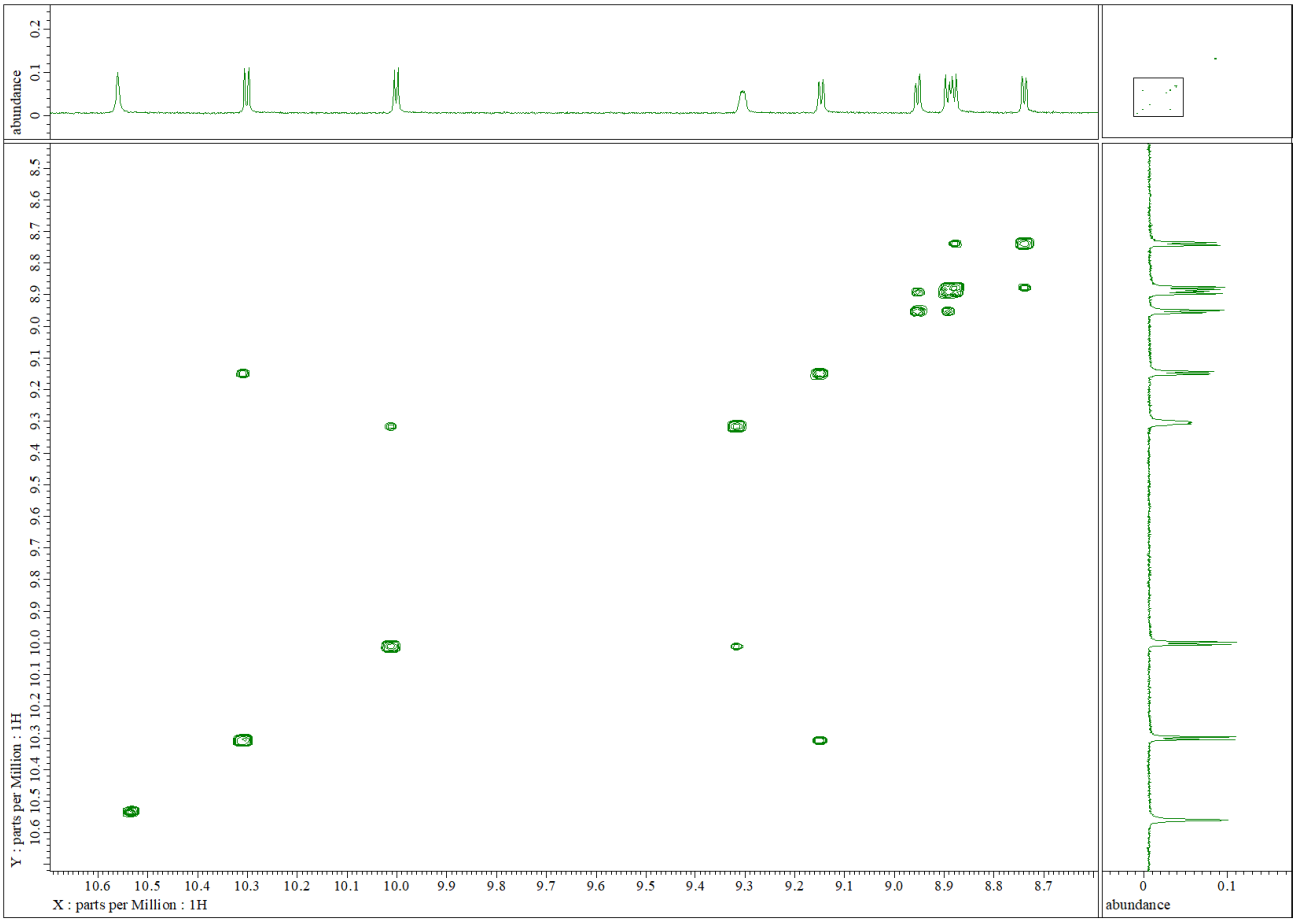

Fig. S2 ^{1}H-^{1}H COSY chart of **5** in $CDCl_3$ at room temperature.

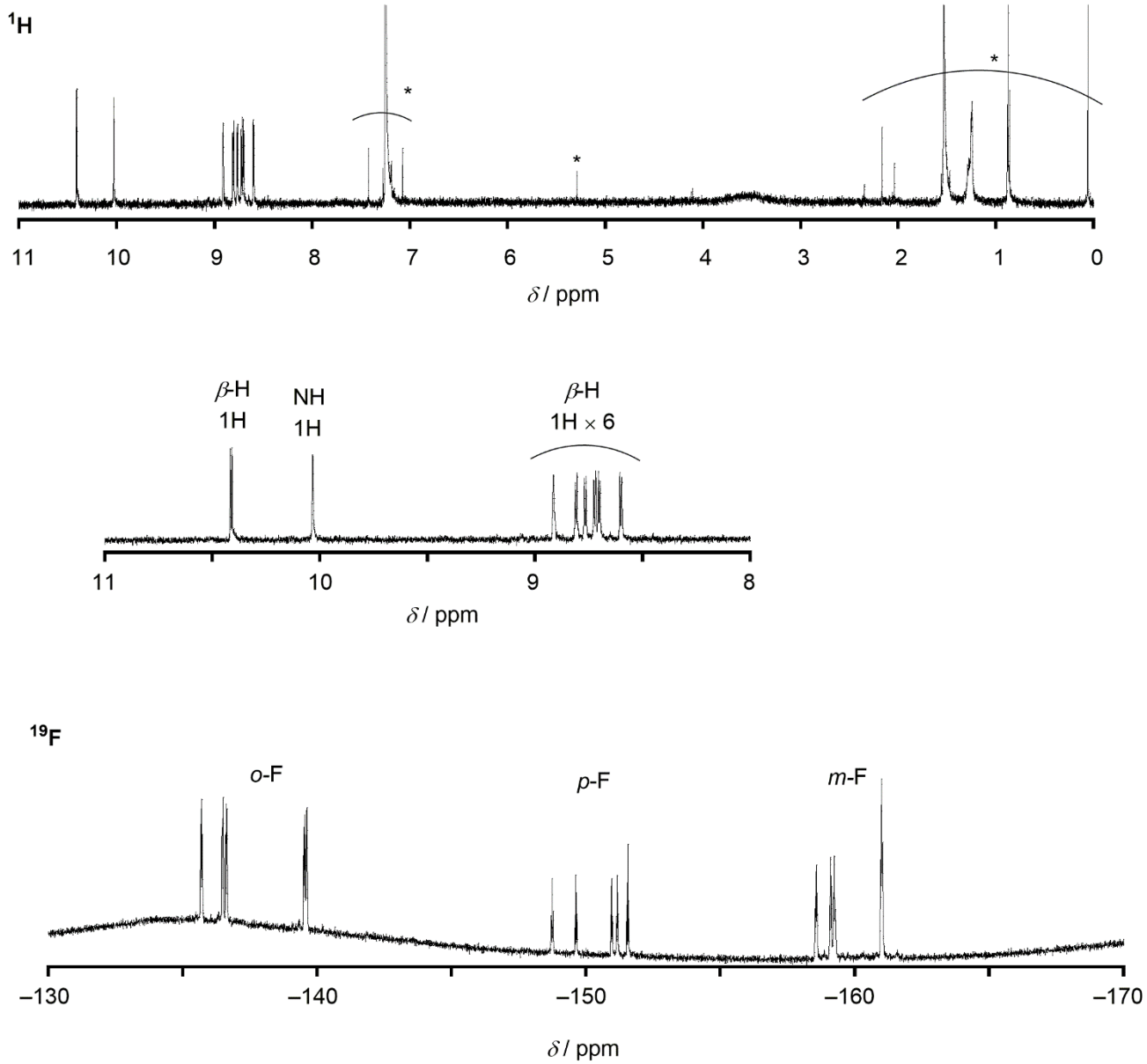

Fig. S3 ^{1}H and ^{19}F NMR spectra of **6** in $CDCl_3$ at room temperature. Peaks marked with * are due to residual solvents and impurities.

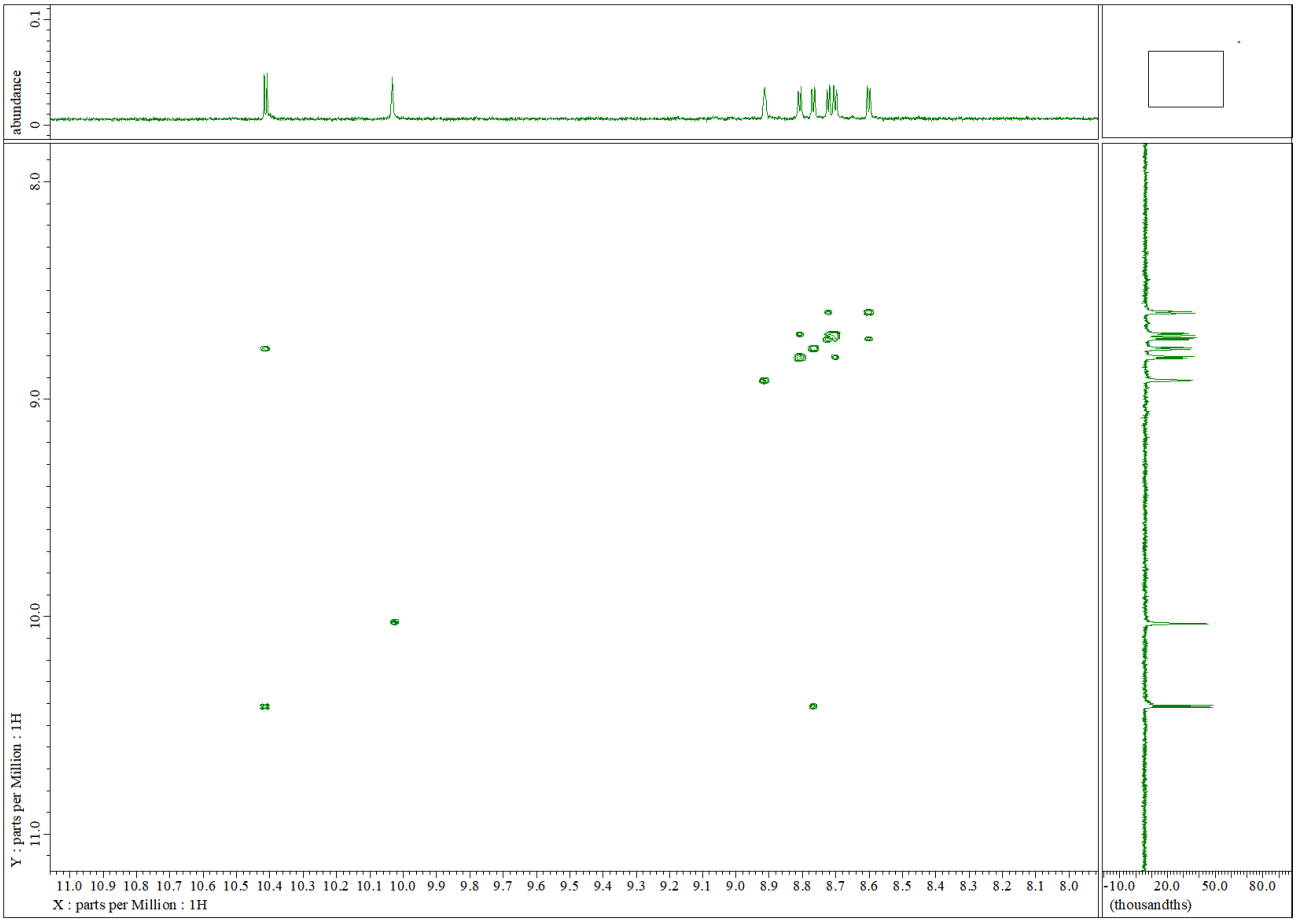

Fig. S4 ^{1}H-^{1}H COSY chart of **6** in $CDCl_3$ at room temperature.

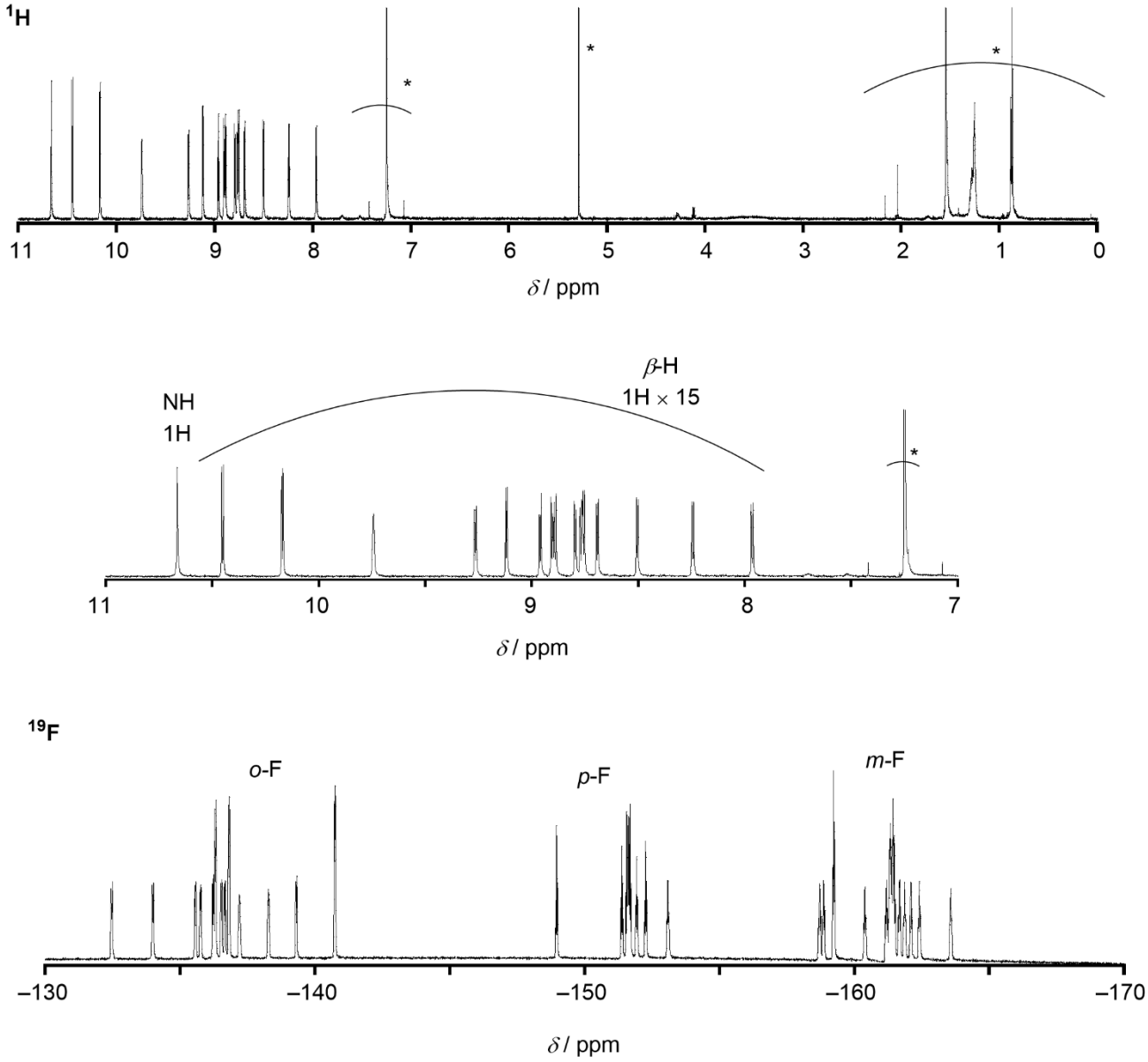

Fig. S5 ^{1}H and ^{19}F NMR spectra of **7** in $CDCl_3$ at room temperature. Peaks marked with * are due to residual solvents and impurities.

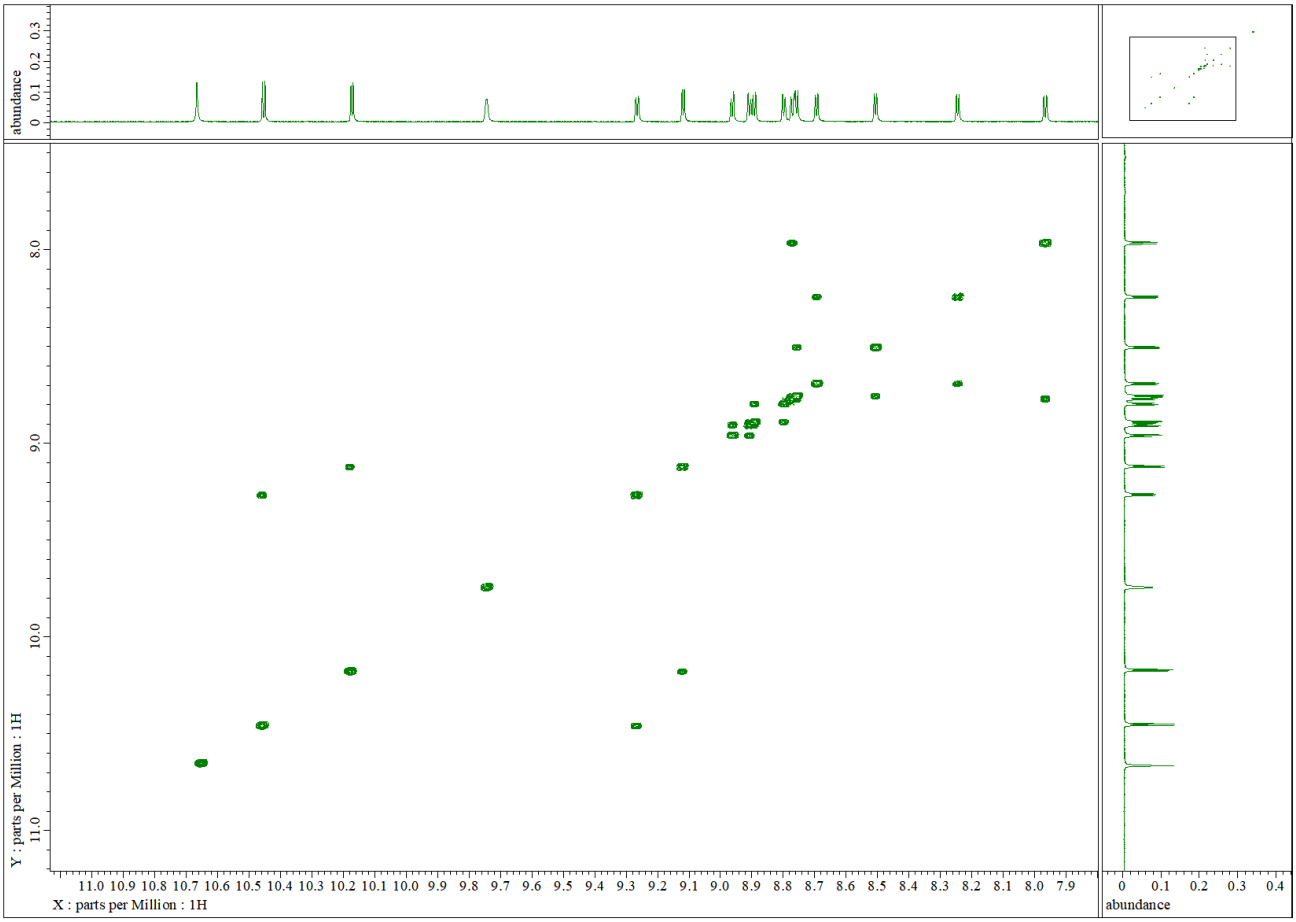

Fig. S6 ^{1}H-^{1}H COSY chart of **7** in $CDCl_3$ at room temperature.

4. HR mass spectra

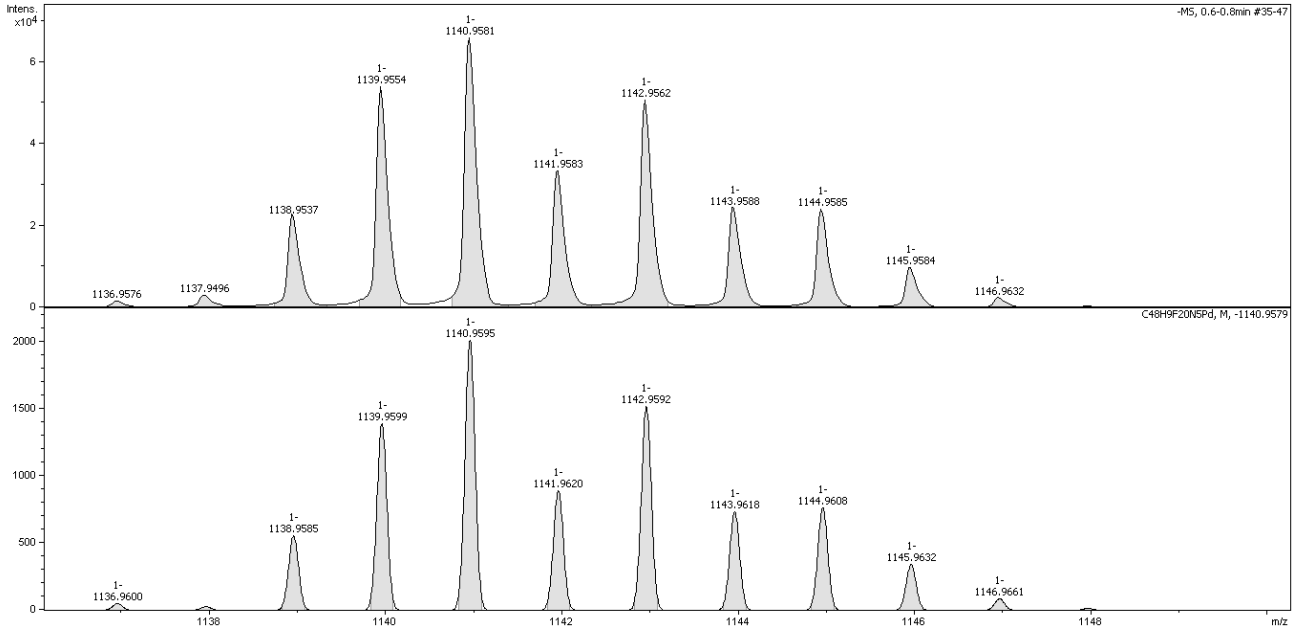

Fig. S7 Observed (top) and simulated (bottom) HR APCI-TOF-MS spectra of **5**.

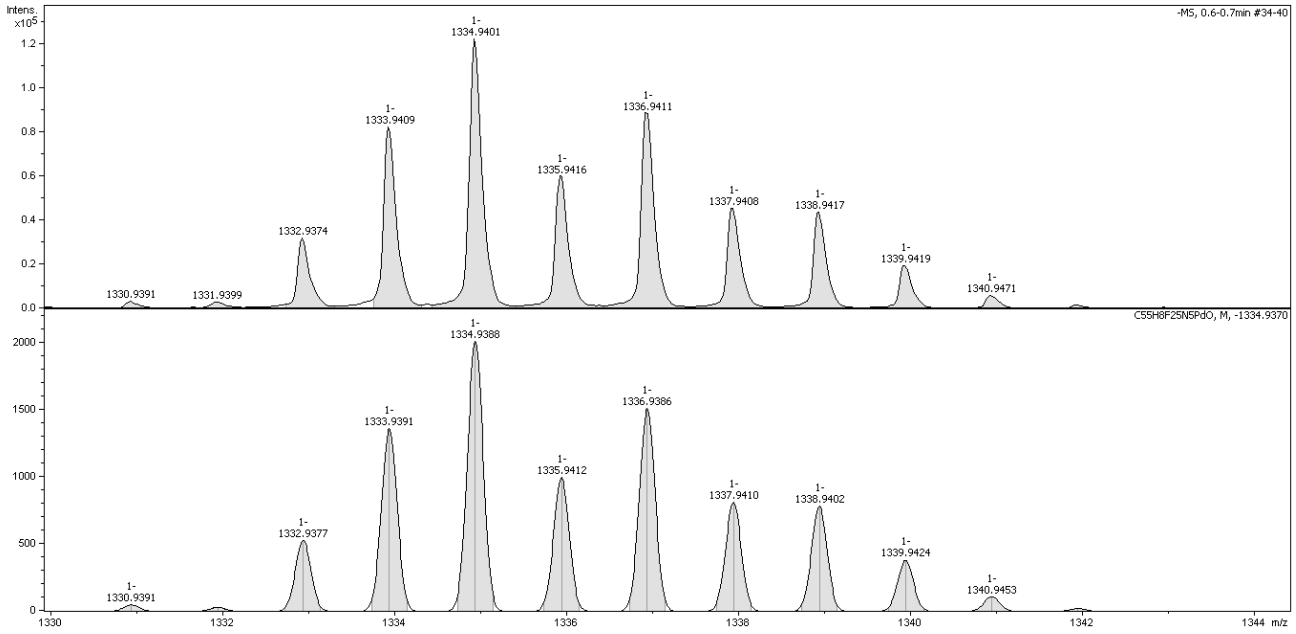

Fig. S8 Observed (top) and simulated (bottom) HR APCI-TOF-MS spectra of **6**.

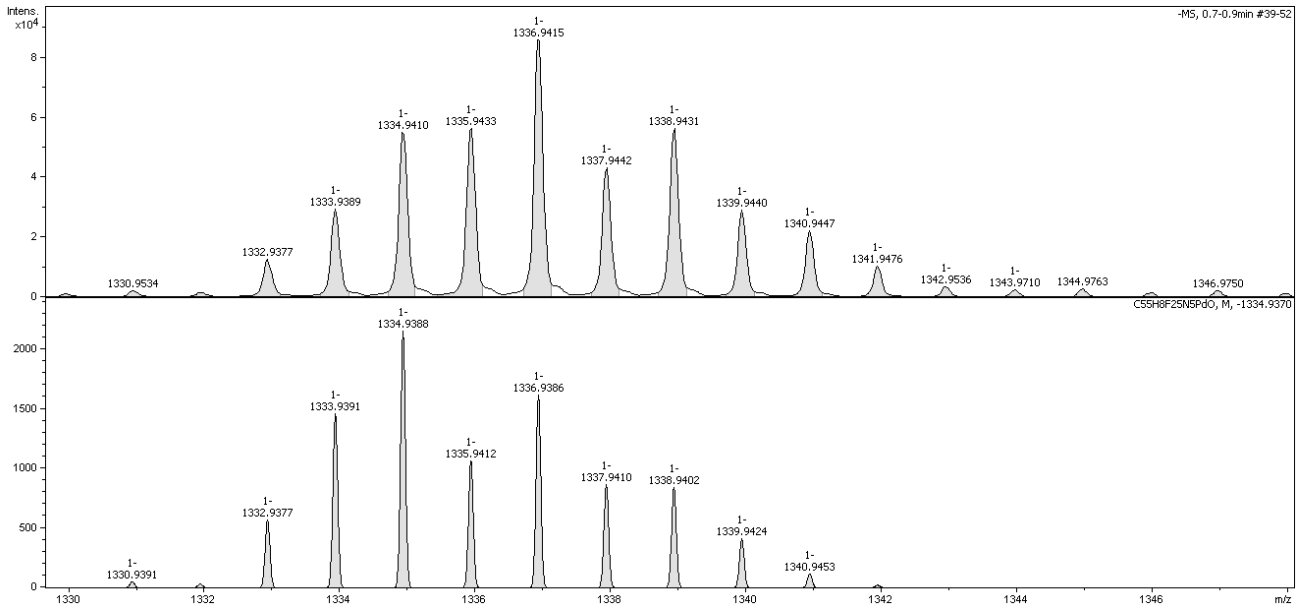

Fig. S9 Observed (top) and simulated (bottom) HR APCI-TOF-MS spectra of **6**. The observed spectrum was obtained from the reaction in the presence of small amount of $H_2{}^{18}O$, wherein two mass differences were detected relative to the calculated spectrum, which suggests that the oxygen atom came from the adventitious water.

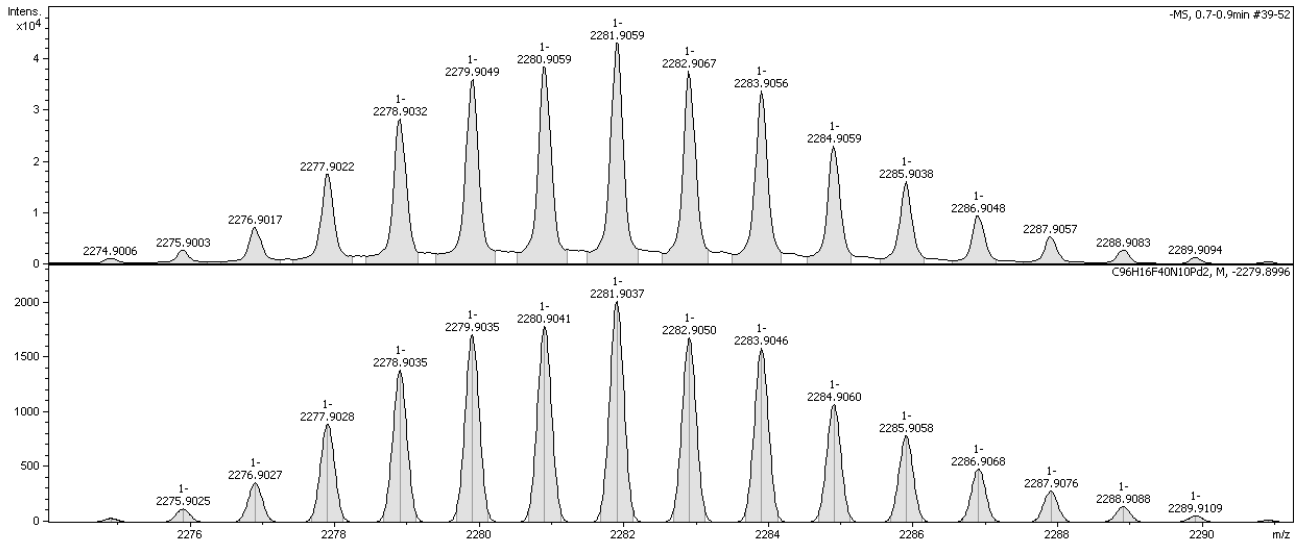

Fig. S10 Observed (top) and simulated (bottom) HR APCI-TOF-MS spectra of **7**.

5. Electrochemical properties

(a)

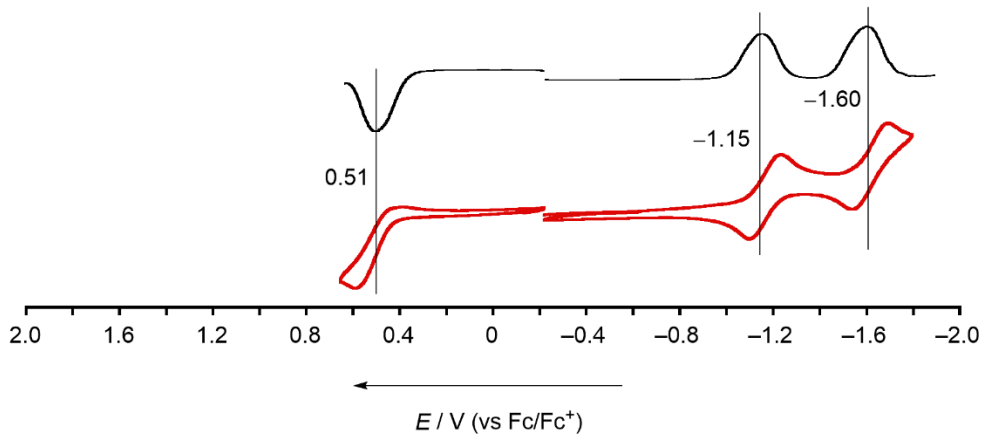

(b)

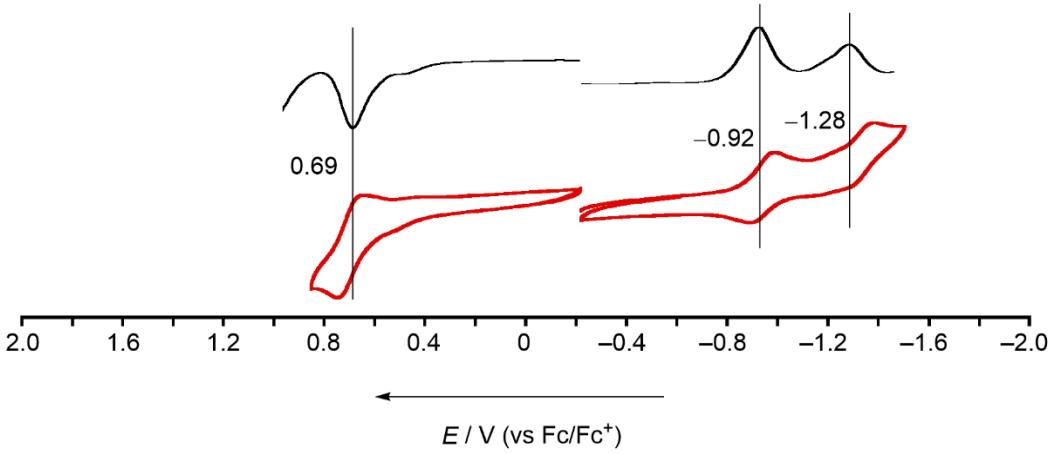

(c)

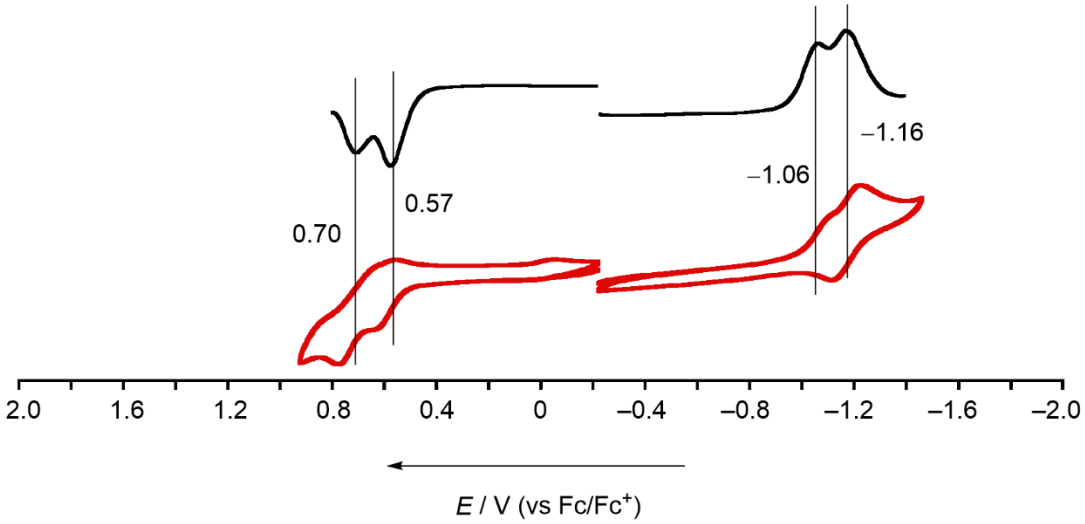

Fig. S11 Cyclic voltammograms of (a) **5**, (b) **6** and (c) **7**. Differential pulse voltammograms are also shown. Measurement conditions: solvent: CH_2Cl_2; scan rate: 0.05 V/s; working electrode: Pt; reference electrode: $Ag/AgNO_3$; counter electrode: Pt; electrolyte: 0.1 M *n*-Bu_4NPF_6.

6. Crystallographic data

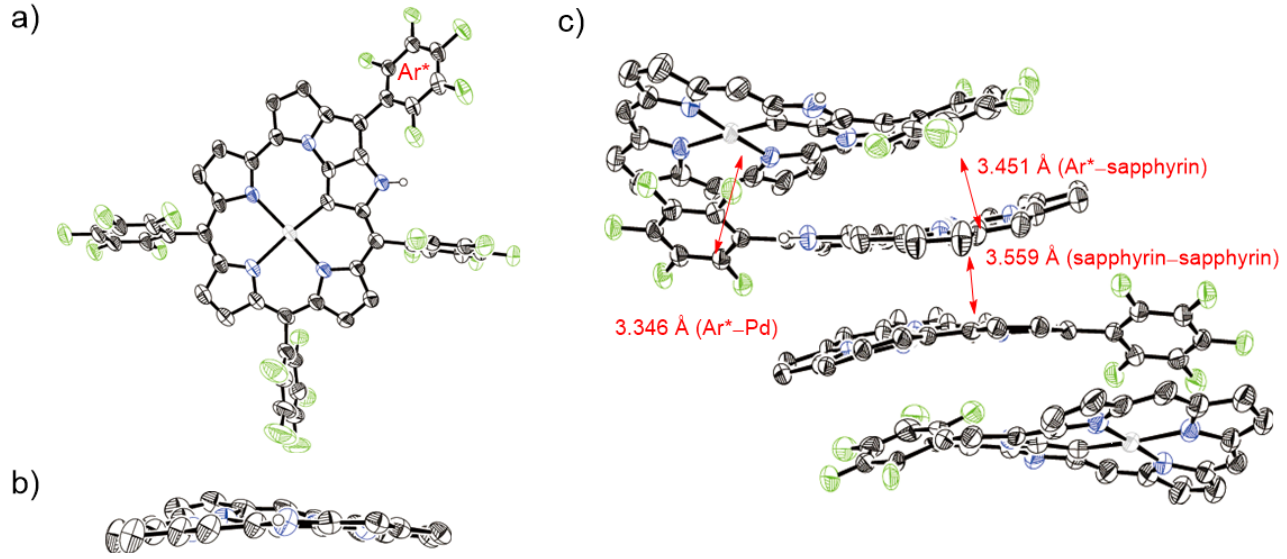

Fig. S12 X-Ray crystal structure of **5** (a) top view, (b) side view, and (c) packing structure. The thermal ellipsoids are 50% probability. One of two independent molecules is shown for (a) and (b). Solvent molecules, pentafluorophenyl groups (side view and packing structure) and hydrogen atoms except for NHs are partially omitted for clarity.

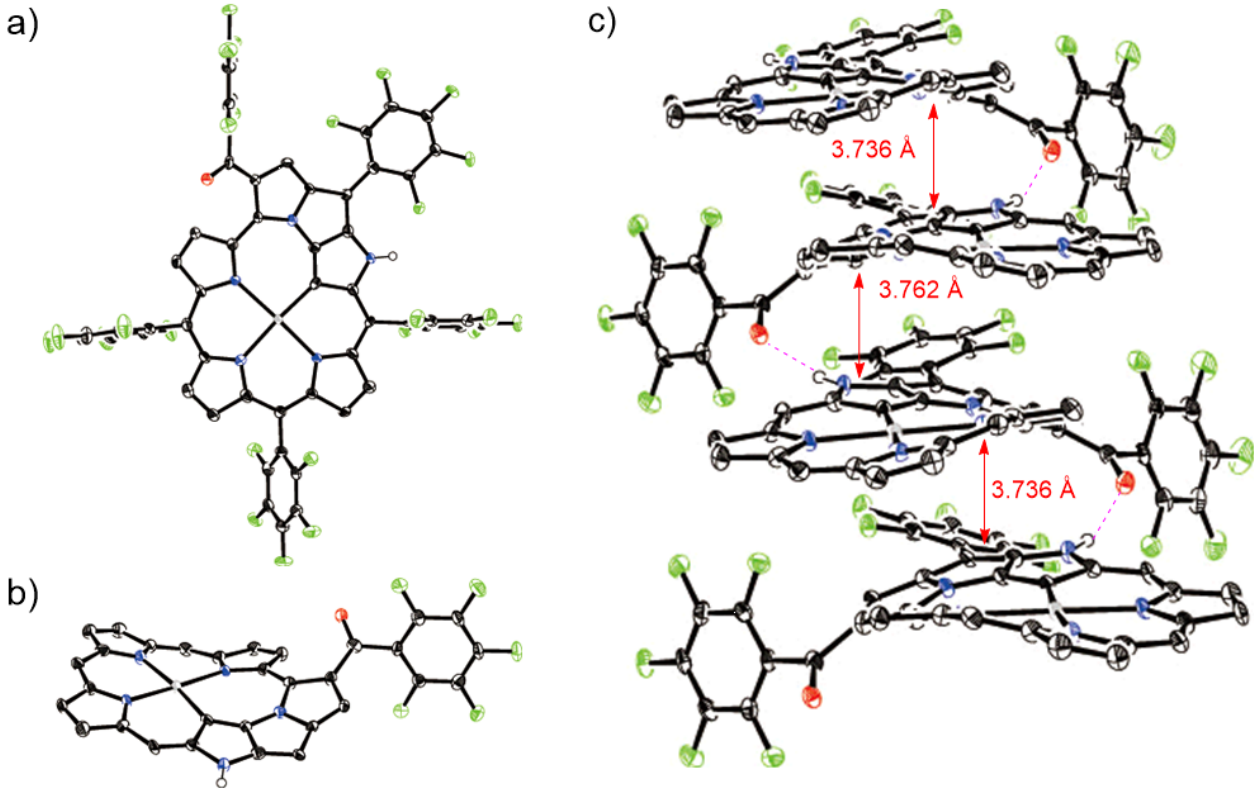

Fig. S13 X-Ray crystal structure of **6** (a) top view, (b) side view, and (c) packing structure. The thermal ellipsoids are 50% probability. One of two independent molecules is shown for (a) and (b). Solvent molecules, pentafluorophenyl groups (side view and packing structure) and hydrogen atoms except for NHs are partially omitted for clarity. Pink dashed lines indicate hydrogen bonding networks.

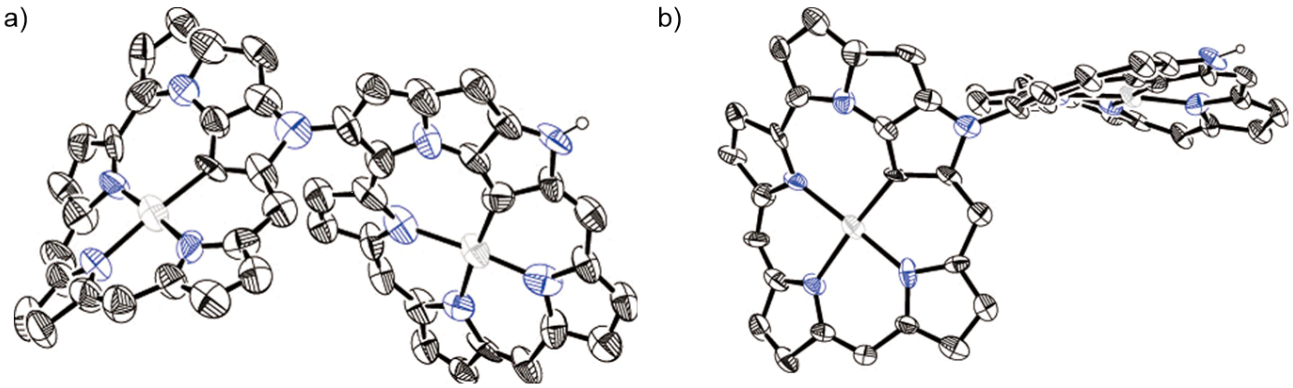

Fig. S14 Preliminary X-ray crystal structure of **7** (a) perspective view and (b) top view. The thermal ellipsoids are 25% probability. One of two independent molecules is shown. Pentafluorophenyl groups and hydrogen atoms except for NHs are omitted for clarity.

Table S1. Crystallographic data for **5**, **6** and **7**.

	5	**6**	**7** [a]
formula	$C_{48}H_{21}F_{20}N_5Pd$, 2(C_3H_6O)	2($C_{55}H_8F_{25}N_5OPd$), $C_2H_4Cl_2$	$C_{96}H_{16}F_{40}N_{10}Pd_2$
solvent	acetone, MeOH / H_2O	1,2-DCE / *n*-hexane	MeCN, MeOH / H_2O
M_r	1258.16	2771.08	2281.99
T[K]	93	93	93
crystal system	triclinic	triclinic	triclinic
space group	*P*-1 (No.2)	*P*-1 (No.2)	*P*-1 (No.2)
a [Å]	16.800(3)	11.5850(19)	18.2349(7)
b [Å]	17.172(2)	17.0459(19)	22.6345(9)
c [Å]	18.1752(18)	25.259(3)	22.723(1)
α [°]	64.83(2)	74.717(7)	77.441(4)
β [°]	85.41(4)	88.666(14)	86.990(3)
γ [°]	83.23(4)	85.041(12)	79.486(3)
V [Å^3]	4709.8(14)	4793.7(11)	8999.7(7)
Z	4	4	4
ρ_{calcd} [g / cm^3]	1.774	1.920	1.684
R_1 [$I > 2\sigma(I)$]	0.0763	0.0496	0.1328
wR_2 (all data)	0.2116	0.1218	0.3892
GOF [$I > 2\sigma(I)$]	1.052	1.009	1.219
CCDC No.	2058737	2058736	2058738

a: The contributions to the scattering arising from the presence of the disordered solvents in the crystal were removed by use of the utility *SQUEEZE* in the PLATON software package. [S2]

7. Plausible reaction mechanism

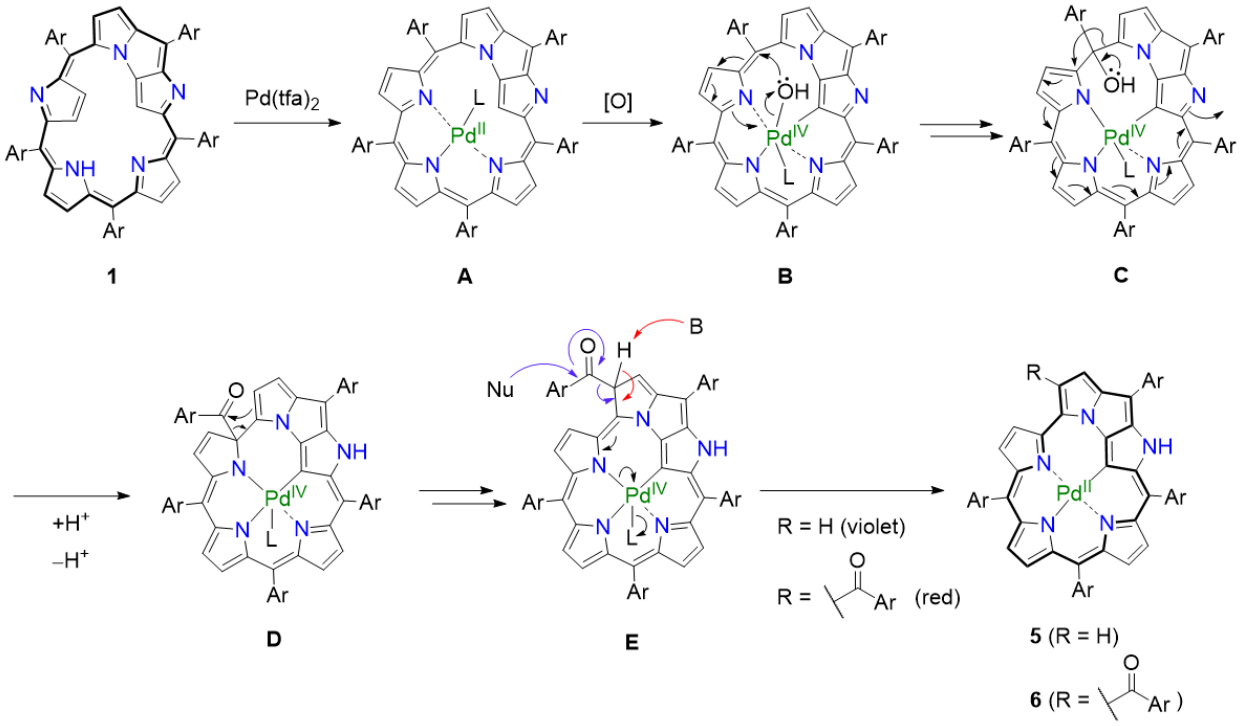

Scheme S1. A possible reaction route from **1** to **5** or **6**. Ar = pentafluorophenyl. L = CF_3COO^-, B = base, and Nu = nucleophile in the system.

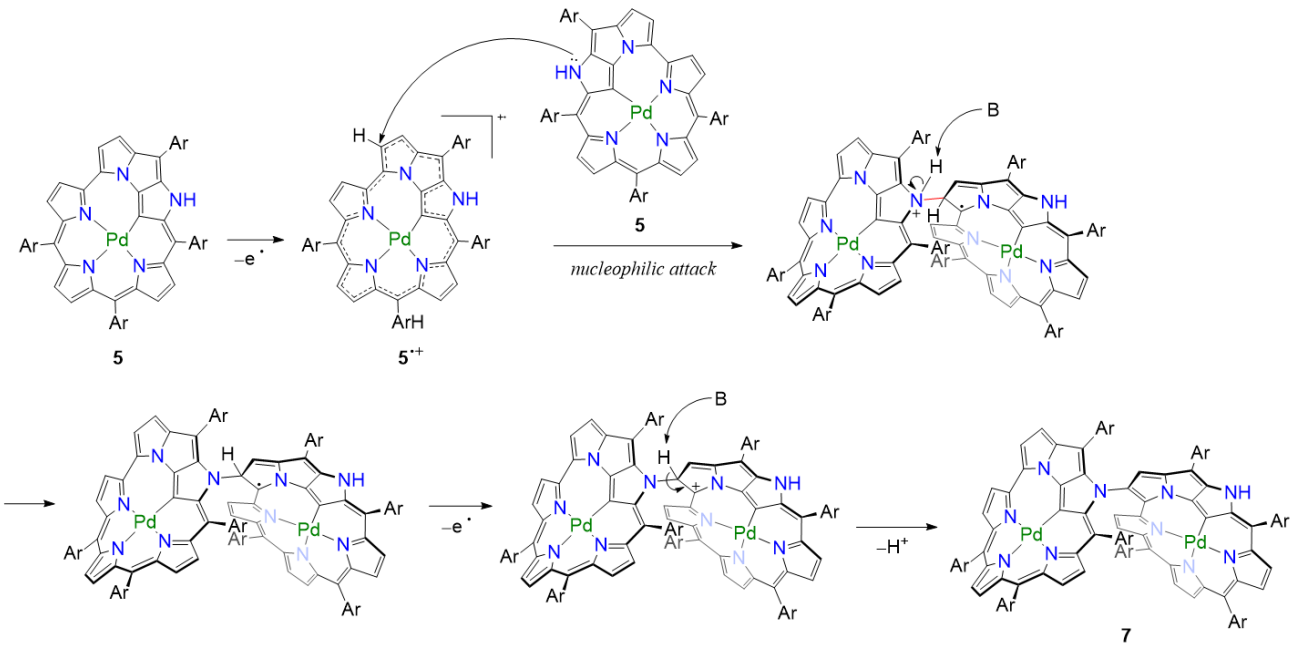

Scheme S2. A possible reaction route from **5** to **7**. B = base in the system.

8. DFT calculations

All calculations were carried out using the *Gaussian 16* program.[S3] All structures were fully optimized without any symmetry restriction. The calculations were performed by the density functional theory (DFT) method with restricted B3LYP (Becke's three-parameter hybrid exchange functionals and the Lee-Yang-Parr correlation functional) level, employing a basis set 6-31G(d) for C, H, N, O, F and LANL2DZ for Pd. The NICS values and absolute ^{1}H shielding values were obtained with the GIAO method, employing a basis set 6-31G(d) for C, H, N, F and LANL2DZ for Pd. The ^{1}H chemical shift values were calculated relative to $CHCl_3$ (δ = 7.26 ppm, absolute shielding: 24.94 ppm). The global ring centers for the NICS values were designated at the nonweighted means of the carbon and nitrogen coordinates on the peripheral positions of conjugated macrocycles. In addition, NICS values were also calculated on centers of other local cyclic structures as depicted in the figures. Spin density distributions have been calculated at the UB3LYP/6-31G(d) for C, H, N, F and LANL2DZ for Pd.

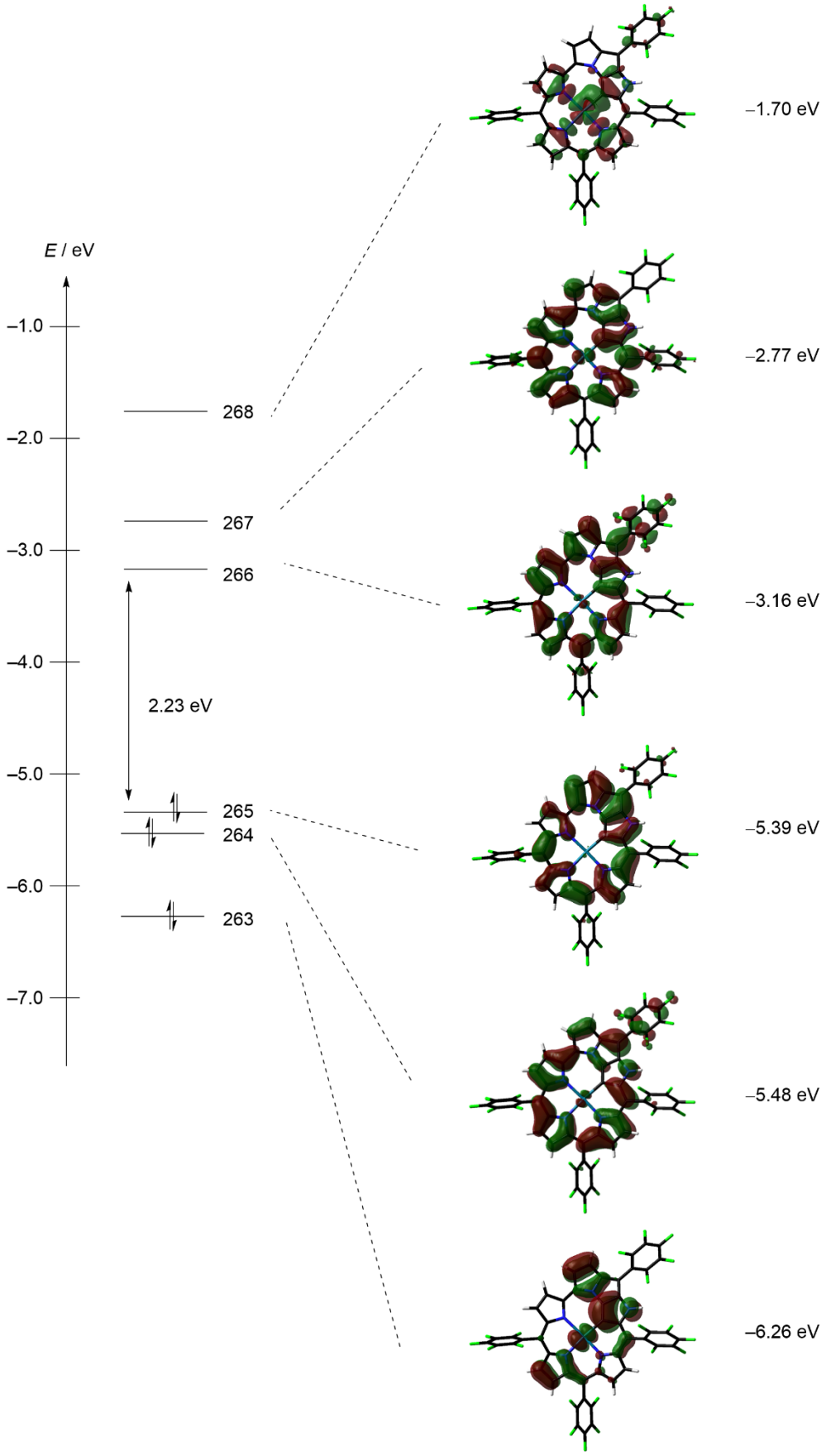

Fig. S15 Kohn–Sham orbital diagrams of **5**.

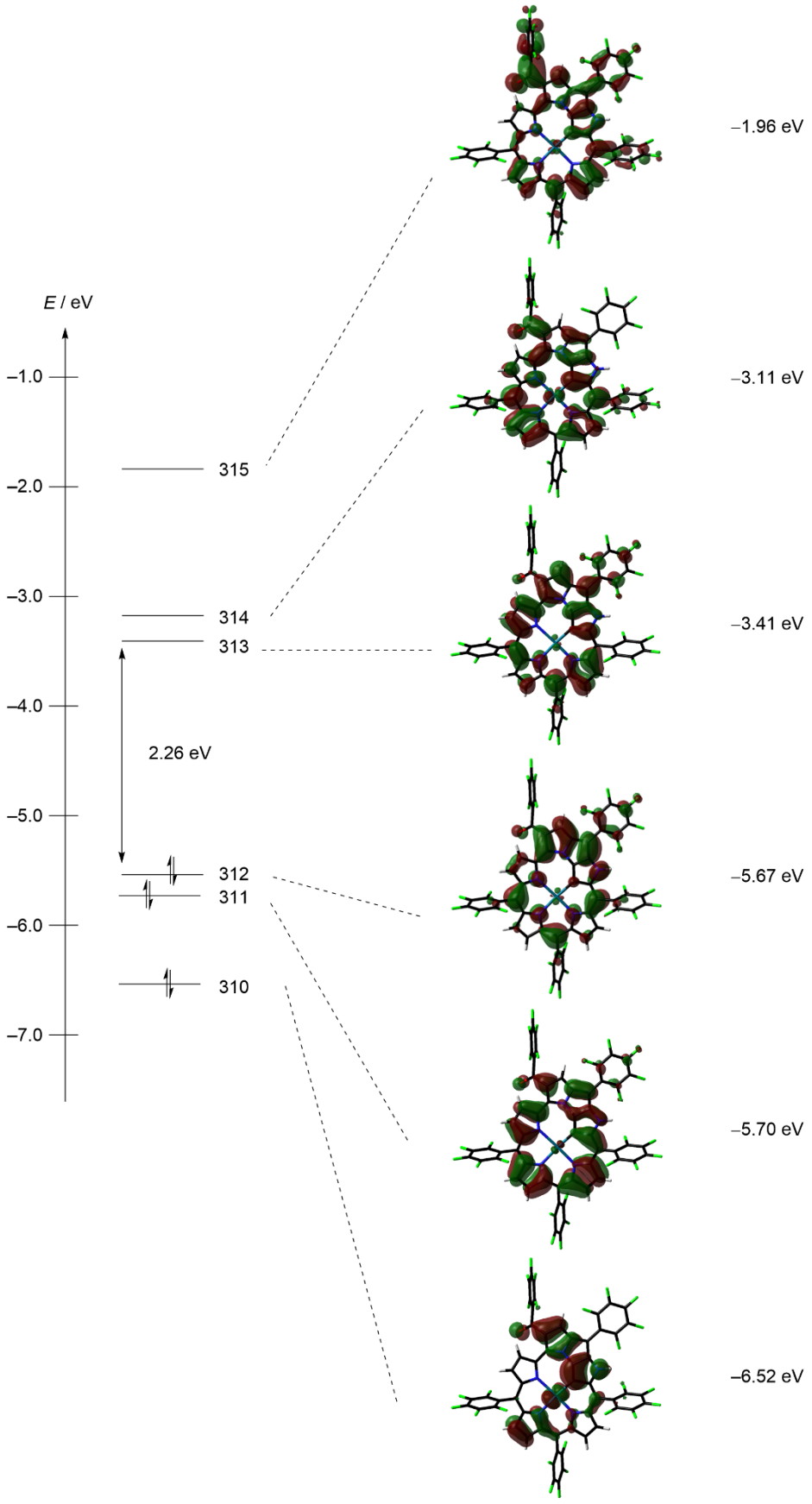

Fig. S16 Kohn–Sham orbital diagrams of **6**.

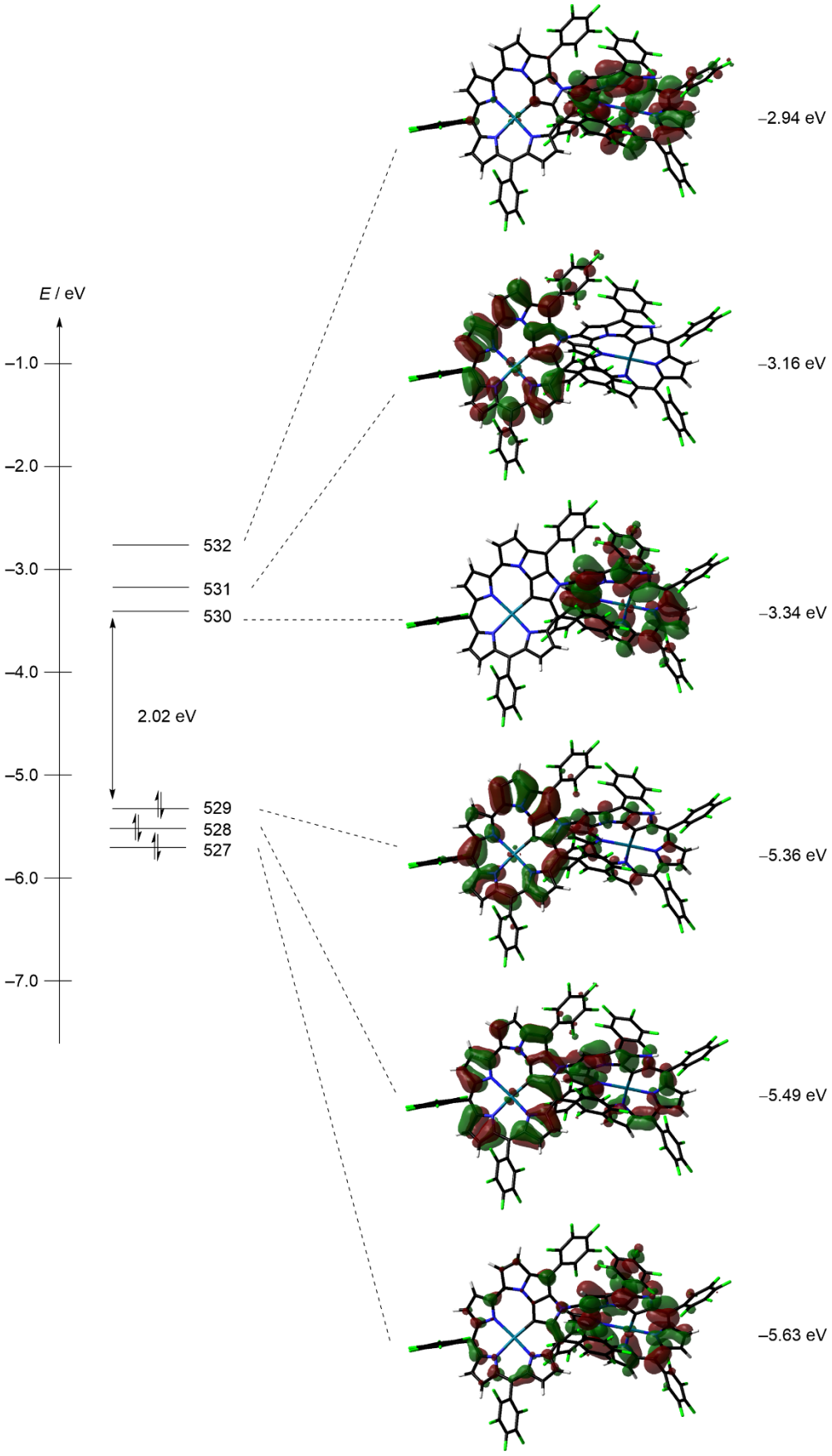

Fig. S17 Kohn–Sham orbital diagrams of **7**.

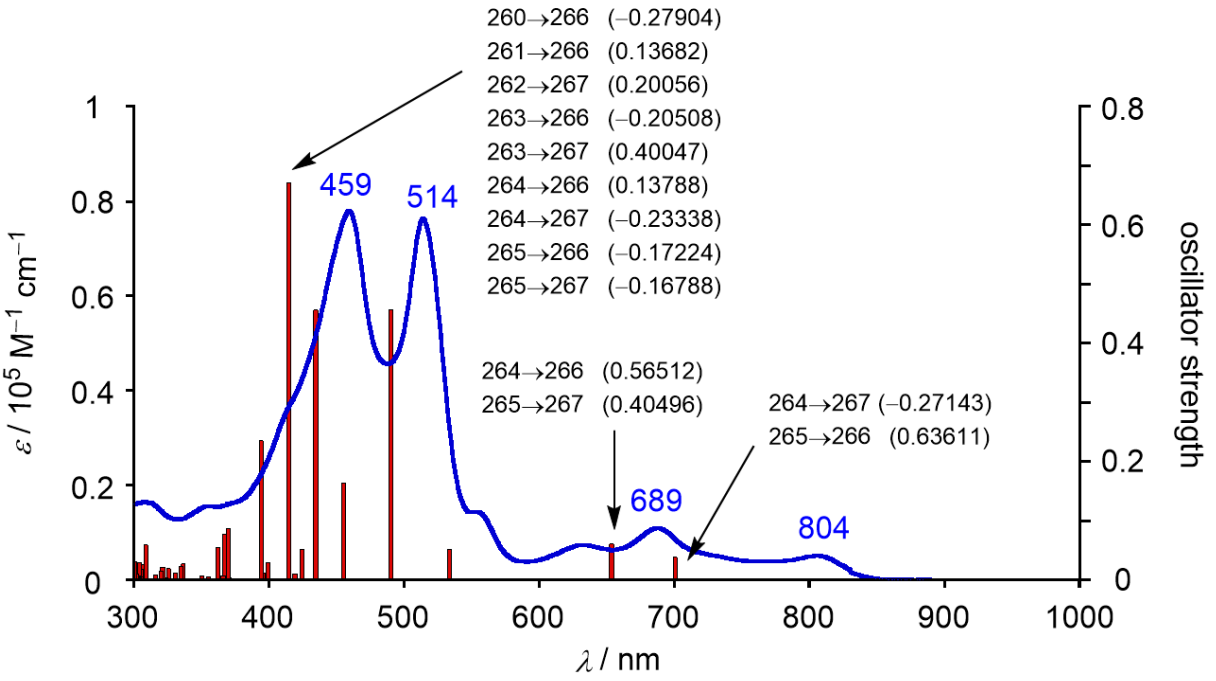

Fig. S18 Calculated absorption spectrum of **5** on the basis of optimized structure (red bar), observed absorption spectrum (blue line). Selected oscillator strengths: f = 0.0391 (700 nm), 0.0609 (653 nm), 0.4570 (489 nm), 0.4583 (434 nm), and 0.6710 (414 nm).

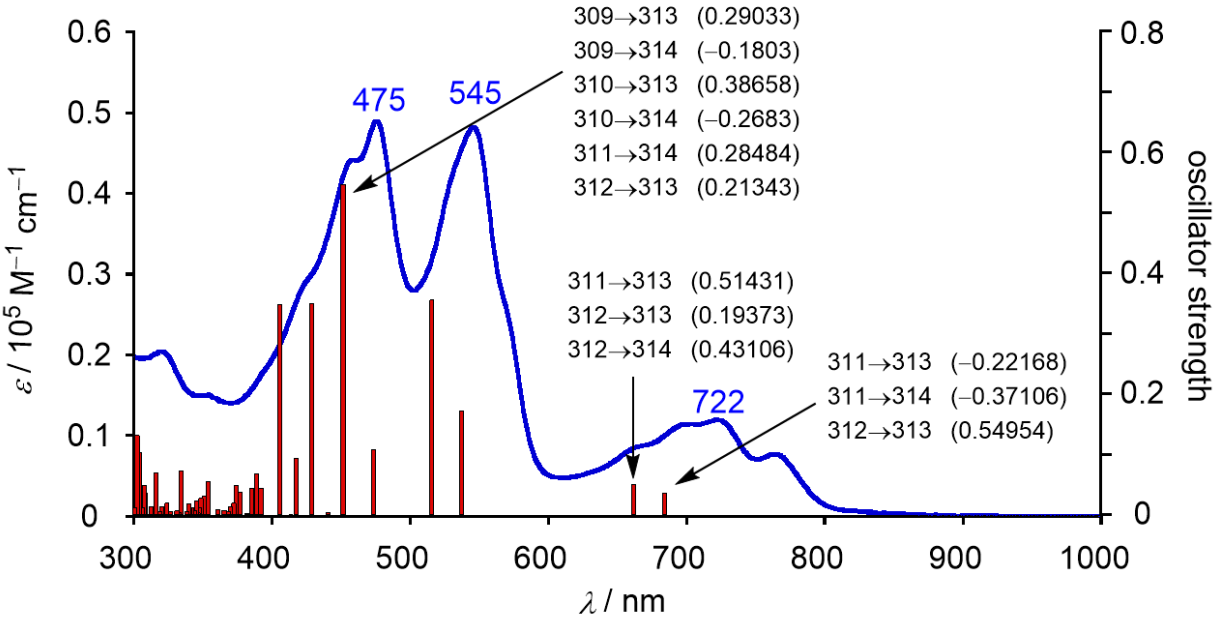

Fig. S19 Calculated absorption spectrum of **6** on the basis of optimized structure (red bar), observed absorption spectrum (blue line). Selected oscillator strengths: f = 0.0361 (684 nm), 0.0501 (662 nm), 0.3557 (515 nm), 0.5473 (451 nm), 0.3502 (429 nm) and 0.3488 (406 nm).

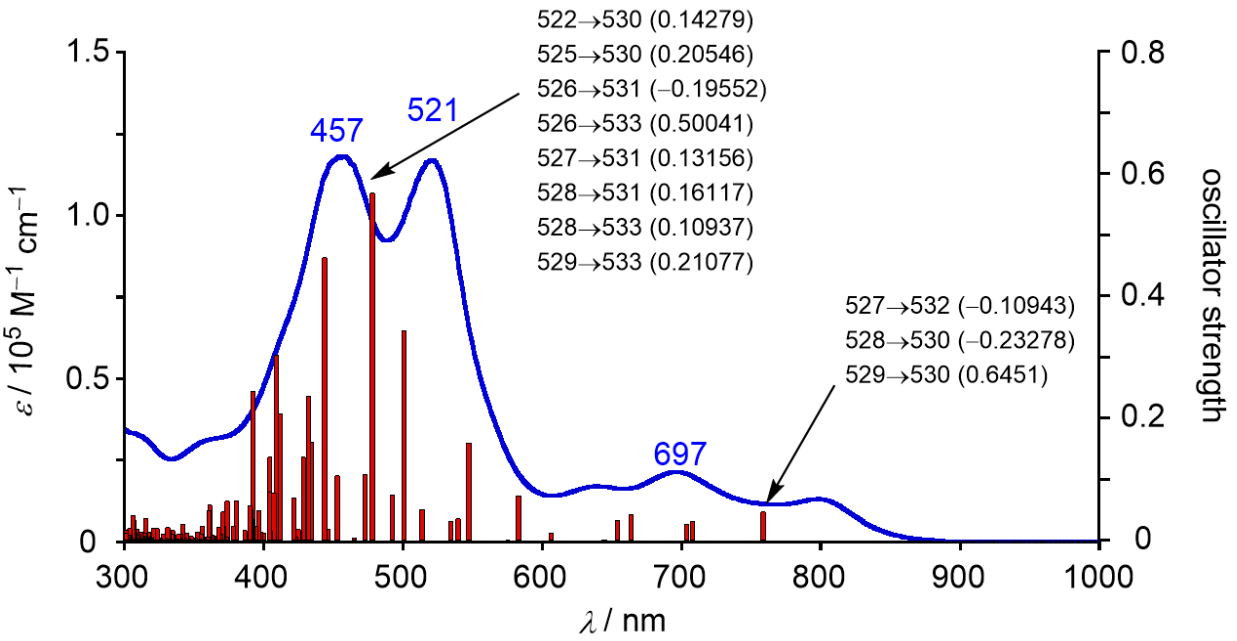

Fig. S20 Calculated absorption spectrum of **7** on the basis of optimized structure (red bar), observed absorption spectrum (blue line). Selected oscillator strengths: f = 0.0468 (759 nm), 0.0314 (708 nm), 0.0271 (704 nm), 0.3430 (501 nm), 0.5687 (478 nm) and 0.4631 (444 nm).

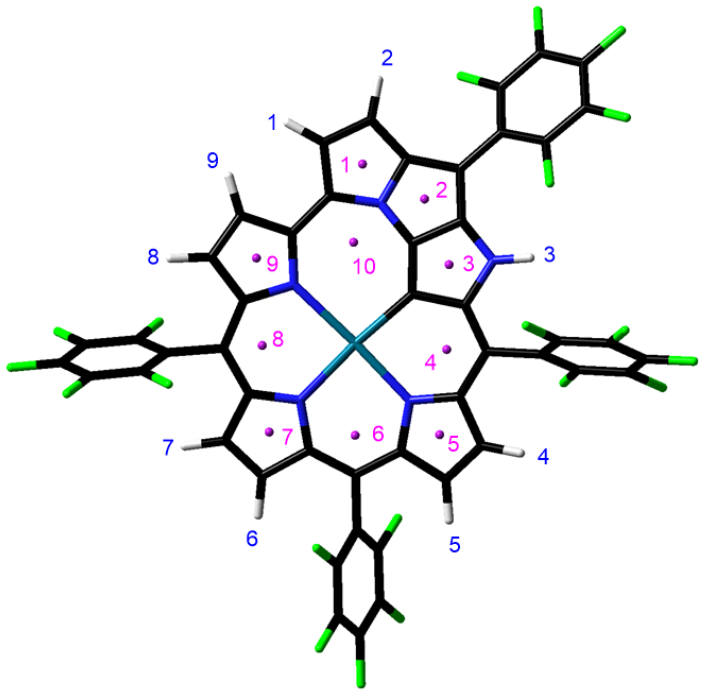

position	NICS (ppm)	^{1}H	δ (ppm)
1	–19.52	1	10.11
2	–21.82	2	9.58
3	–8.57	3	10.30
4	–20.31	4	8.86
5	–6.43	5	8.91
6	–19.89	6	8.80
7	–4.61	7	8.59
8	–20.66	8	9.14
9	–4.71	9	10.23
10	–16.17		

Fig. S21 NICS(0) values at selected points and simulated chemical shifts of **5**.

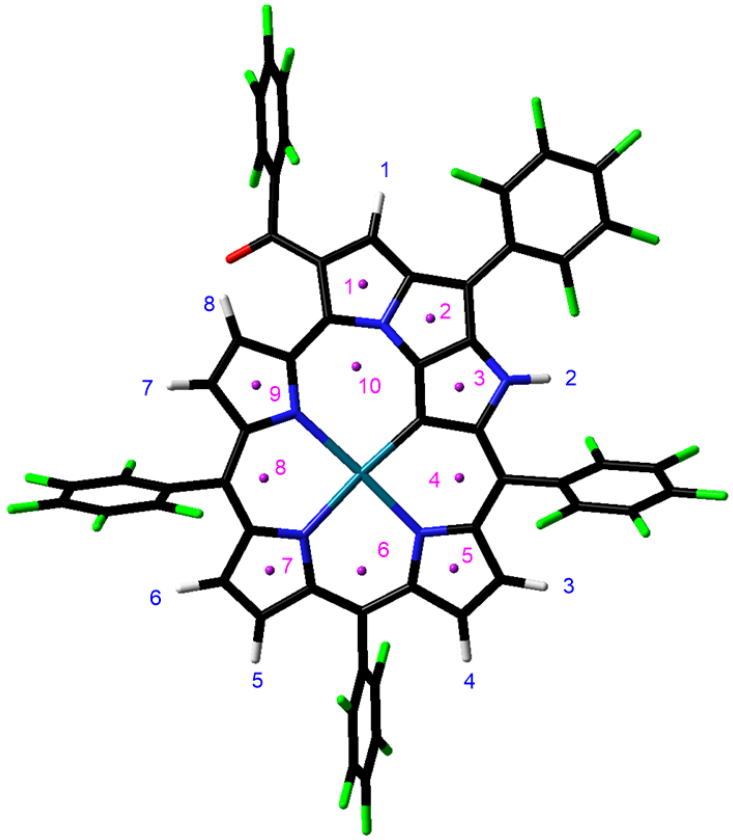

position	NICS (ppm)	^{1}H	δ (ppm)
1	–16.23	1	9.10
2	–16.76	2	9.90
3	–4.61	3	8.63
4	–18.85	4	8.70
5	–5.66	5	8.71
6	–18.05	6	8.46
7	–4.52	7	8.75
8	–18.81	8	10.54
9	–4.99		
10	–15.61		

Fig. S22 NICS(0) values at selected points and simulated chemical shifts of **6**.

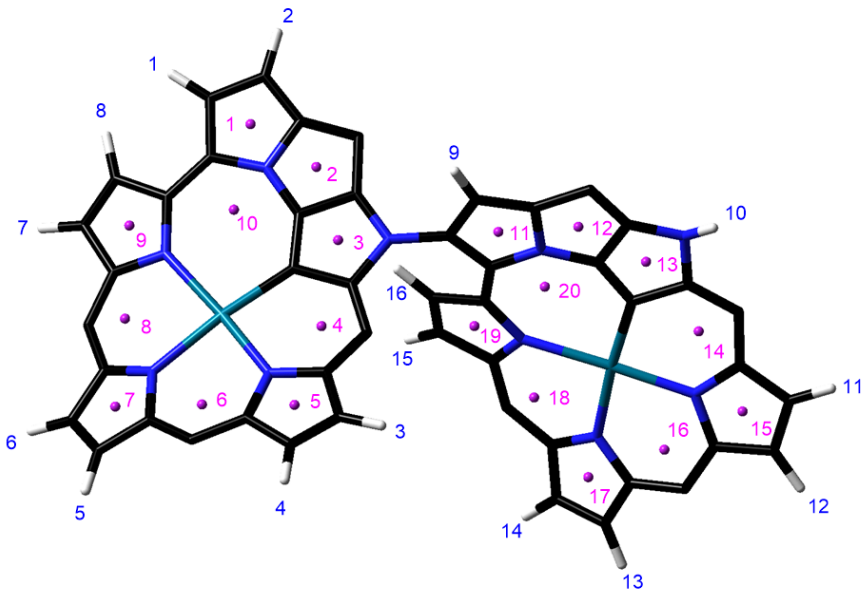

position	NICS (ppm)	^{1}H	δ (ppm)
1	–18.61	1	10.21
2	–20.58	2	9.59
3	–6.38	3	7.44
4	–20.23	4	8.45
5	–6.85	5	8.72
6	–19.69	6	8.78
7	–4.77	7	9.28
8	–20.22	8	10.41
9	–4.92	9	10.09
10	–15.51	10	10.35
11	–18.50	11	8.78
12	–19.33	12	8.79
13	–5.90	13	8.63
14	–18.86	14	8.19
15	–5.86	15	7.54
16	–18.37	16	8.19
17	–4.86		
18	–19.49		
19	–5.77		
20	–15.79		

Fig. S23 NICS(0) values at selected points and simulated chemical shifts of **7**. *meso*-Pentafluorophenyl groups are not shown in this figure for clarity.

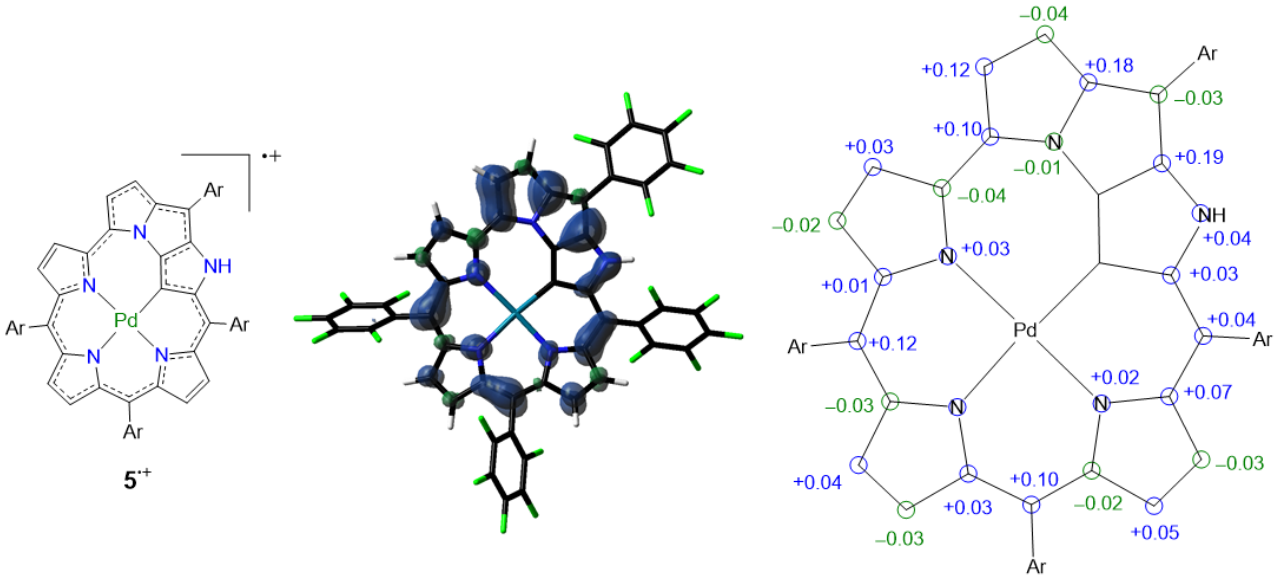

Fig. S24 Calculated spin density of $\mathbf{5}^{\bullet+}$ (isovalue: 0.0015).

9. References

[S1] For SHELEXT-2014/5 and SHELEXL-2014/7, programs for refinement of crystal structure from diffraction data, University of Göttingen (Germany), see: a) G. Sheldrick, T. Schneider, *Methods Enzymol.*, 1997, **277**, 319. b) G. M. Sheldrick, *Acta Cryst.*, 2008, **A64**, 112. c) G. M. Sheldrick, *Acta Cryst.*, 2015, **A71**, 3. d) G. M. Sheldrick, *Acta Cryst.*, 2015, **C71**, 3.

[S2] A. L. Spek, *PLATON, A Multipurpose Crystallographic Tool*, Utrecht University, Utrecht, The Netherlands, 2005; P. van der Sluis and A. L. Spek, *Acta Crystallogr. Sect. A*, 1990, **46**, 194.

[S3] Gaussian 16, Revision A.03, M. J. Frisch, G. W. Trucks, H. B. Schlegel, G. E. Scuseria, M. A. Robb, J. R. Cheeseman, G. Scalmani, V. Barone, G. A. Petersson, H. Nakatsuji, X. Li, M. Caricato, A. Marenich, J. Bloino, B. G. Janesko, R. Gomperts, B. Mennucci, H. P. Hratchian, J. V. Ortiz, A. F. Izmaylov, J. L. Sonnenberg, D. Williams-Young, F. Ding, F. Lipparini, F. Egidi, J. Goings, B. Peng, A. Petrone, T. Henderson, D. Ranasinghe, V. G. Zakrzewski,J. Gao, N. Rega, G. Zheng, W. Liang, M. Hada, M. Ehara, K. Toyota, R. Fukuda, J. Hasegawa, M. Ishida, T. Nakajima, Y. Honda, O. Kitao, H. Nakai, T. Vreven, K. Throssell, J. A. Montgomery, Jr., J. E. Peralta, F. Ogliaro, M. Bearpark, J. J. Heyd, E. Brothers, K. N. Kudin, V. N. Staroverov, T. Keith, R. Kobayashi, J. Normand, K. Raghavachari, A. Rendell, J. C. Burant, S. S. Iyengar, J. Tomasi, M. Cossi, J. M. Millam, M. Klene, C. Adamo, R. Cammi, J. W. Ochterski, R. L. Martin, K. Morokuma, O. Farkas, J. B. Foresman and D. J. Fox, Gaussian, Inc., Wallingford CT, 2016.